HAL
open science

Ground-based HCN submillimetre measurements in Titan's atmosphere: an intercomparison with Herschel observations

M. Rengel, D. Shulyak, P. Hartogh, H. Sagawa, R. Moreno, C. Jarchow, D. Breitschwerdt

To cite this version:

M. Rengel, D. Shulyak, P. Hartogh, H. Sagawa, R. Moreno, et al.. Ground-based HCN submillimetre measurements in Titan's atmosphere: an intercomparison with Herschel observations. Astronomy and Astrophysics - A&A, 2022, 658, 10.1051/0004-6361/202141422 . insu-03713339

HAL Id: insu-03713339
https://insu.hal.science/insu-03713339v1

Submitted on 4 Jul 2022

HAL is a multi-disciplinary open access archive for the deposit and dissemination of scientific research documents, whether they are published or not. The documents may come from teaching and research institutions in France or abroad, or from public or private research centers.

L'archive ouverte pluridisciplinaire **HAL**, est destinée au dépôt et à la diffusion de documents scientifiques de niveau recherche, publiés ou non, émanant des établissements d'enseignement et de recherche français ou étrangers, des laboratoires publics ou privés.

A&A 658, A88 (2022)
https://doi.org/10.1051/0004-6361/202141422
© M. Rengel et al. 2022

Astronomy & Astrophysics

Ground-based HCN submillimetre measurements in Titan's atmosphere: an intercomparison with *Herschel* observations*

M. Rengel[1], D. Shulyak[1,2], P. Hartogh[1], H. Sagawa[3], R. Moreno[4], C. Jarchow[1], and D. Breitschwerdt[5]

[1] Max-Planck-Institut für Sonnensystemforschung, Justus-von-Liebig-Weg 3, 37077 Göttingen, Germany
e-mail: rengel@mps.mpg.de
[2] Instituto de Astrofísica de Andalucía - CSIC, c/ Glorieta de la Astronomía s/n, 18008 Granada, Spain
[3] Faculty of Science, Kyoto Sangyo University, Kyoto 603-8555, Japan
[4] LESIA – Observatoire de Paris, CNRS, Université Paris 6, Université Paris-Diderot, 5 place Jules Janssen, 92195 Meudon, France
[5] Zentrum für Astronomie und Astrophysik, Technische Universität Berlin, Hardenbergstrasse 36, 10623 Berlin, Germany

Received 28 May 2021 / Accepted 25 November 2021

ABSTRACT

Aims. The aim of this study is to measure the vertical distribution of HCN on Titan's stratosphere using ground-based submillimetre observations acquired quasi-simultaneously with the *Herschel* ones. This allows us to perform a consistency check between space and ground-based observations and to build a reference mean HCN vertical profile in Titan's stratosphere.

Methods. Using APEX and IRAM 30-m, we obtained the spectral emission of HCN (4-3) and (3-2) lines. Observations were reduced with GILDAS-CLASS. We applied a line-by-line radiative transfer code to calculate the synthetic spectra of HCN, and a retrieval algorithm based on optimal estimation to retrieve the temperature and HCN vertical distributions. We used the standard deviation-based metric to quantify the dispersion between the ground-based and *Herschel* HCN profiles and the mean one.

Results. Our derived HCN abundance profiles are consistent with an increase from 40 ppb at ~100 km to 4 ppm at ~200 km, which is an altitude region where the HCN signatures are sensitive. We also demonstrate that the retrieved HCN distribution is sensitive to the data information and is restricted to Titan's stratosphere. The HCN obtained from APEX data is less accurate than the one from IRAM data because of the poorer data quality, and covers a narrower altitude range. Comparisons between our results and the values from *Herschel* show similar abundance distributions, with maximum differences of 2.5 ppm ranging between 100 and 300 km in the vertical range. These comparisons also allow us to inter-validate both data sets and indicate reliable and consistent measurements. The inferred abundances are also consistent with the vertical distribution in previous observational studies, with the profiles from ALMA, Cassini/CIRS, and SMA (the latest ones below ~230 km). Our HCN profile is also comparable to photochemical models by Krasnopolsky (2014) and Vuitton et al. (2019) below 230 km and consistent with that of Loison et al. (2015) above 250 km. However, it appears to show large differences with respect to the estimates by Loison et al. (2015), Dobrijevic & Loison (2018), and Lora et al. (2018) below 170 km, and by Dobrijevic & Loison (2018) and Lora et al. (2018) above 400 km, although they are similar in shape. We conclude that these particular photochemical models need improvement.

Key words. planets and satellites: atmospheres – planets and satellites: individual: Titan – techniques: spectroscopic

1. Introduction

The atmosphere of Titan, one of the moons of Saturn, is cold, dense, and nitrogen (N_2)-dominated, and exhibits a great diversity of molecules and a complex atmospheric chemistry. Hydrogen cyanide (HCN), a molecule crucial to the production of life's building blocks, is the main nitrile species observed in Titan's atmosphere, and indeed Titan has the most HCN-rich atmosphere in the Solar System. The detection of HCN in Titan's atmosphere is robust and its vertical profile has been determined by spectroscopic observations (Coustenis et al. 1991; Hidayat et al. 1997; Marten et al. 2002; Gurwell 2004; Vinatier et al. 2007; Courtin et al. 2011; Rengel et al. 2011, 2014; Molter et al. 2016; Thelen et al. 2019; Lellouch et al. 2019). HCN is generated photochemically in Titan's atmosphere from reactions of hydrocarbon radicals with atomic nitrogen. The latter is produced from extreme ultraviolet (EUV) or electron impact on N_2, or is possibly liberated as a result of cometary impacts (Sekine et al. 2011). HCN is produced at high altitudes, above 300 km (Lara et al. 1996; Wilson & Atreya 2004) and removed by condensation deeper in the atmosphere, setting up a concentration gradient. A more recent alternative explanation proposed that HCN is thermodynamically generated via shock chemistry under lightning discharges in the low atmosphere (Kovács & Turányi 2010).

HCN composition in Titan's stratosphere has been investigated based on a limited number of high-resolution submillimetre observations performed on June 23 and December 15, 2010, with the *Herschel* Space Observatory (Pilbratt et al. 2010) using the Photodetector Array Camera and Spectrometer (PACS) (Poglitsch et al. 2010), and on July 16, 2010, using the Spectral and Photometric REceiver (SPIRE) (Griffin et al. 2010), within the framework of the guaranteed time key programme "Water and related chemistry in the Solar System" (HssO) (Hartogh et al. 2011). Measured HCN vertical distributions were

* *Herschel* is an ESA space observatory with science instruments provided by European-led Principal Investigator consortia and with important participation from NASA.

Open Access article, published by EDP Sciences, under the terms of the Creative Commons Attribution License (https://creativecommons.org/licenses/by/4.0), which permits unrestricted use, distribution, and reproduction in any medium, provided the original work is properly cited.
Open Access funding provided by Max Planck Society.

consistent with an increase from 40 ppb at ~100 km to ~4 ppm at ~200 km, which is an altitude region where the HCN signatures are sensitive (Courtin et al. 2011; Rengel et al. 2014). In support of *Herschel* observations, we observed Titan from the ground at submillimetre (submm) and mm wavelengths using the 12-m single-dish Atacama Pathfinder Experiment (APEX) telescope located at 5100 m above sea level in the Atacama desert in northern Chile (Güsten et al. 2006) and with the Institut de Radioastronomie Millimetrique (IRAM) 30-m telescope in Granada, Spain. Comparing space-based observations with ground-based ones is important; a quantitative link between the inferred HCN abundances obtained by *Herschel* and ground-based observations is required to assess the quality of the data and to inter-validate them. The ground- and space-based observations were acquired in a time period corresponding to a very small fraction of a Titan year, and therefore we assume in the following analysis that temporal temperature variations are negligible. Here we report the ground-based observations and disk-averaged HCN measurements. Furthermore, the accuracy of the measurements is assessed through comparisons with previous, correlative results from *Herschel* and the literature, and we present a mean HCN profile obtained from our ground-based observations and the *Herschel* ones.

Small planets (radius $R \leq 2\,R_{\oplus}$) are the most common in our Galaxy, and they continue to be discovered and characterised. Studies characterising Titan present an opportunity to investigate the atmospheric properties of analogous objects (Titan-like exoplanets) in order to understand their atmospheric characteristics. Here we also add a discussion about HCN in the atmospheres of exoplanets. Fiducial reference HCN abundances for atmospheric studies of Titan-like exoplanets are needed, and studies assessing whether or not these data sets are suitable for such purposes are essential.

2. Observations and data reduction

2.1. APEX observations

After having demonstrated the capabilities of APEX and of the APEX Swedish Heterodyne Facility Instrument (SHeFI APEX-1 receiver) for atmospheric observations on Titan (Rengel et al. 2011), HCN (4-3) at 345 GHz was observed in Titan's atmosphere on June 16, 2010, at APEX[1]. As the front end for the observations, we used the APEX-2 heterodyne receiver (SHeFI 345 GHz band; Vassilev et al. (2008)). This receiver employs superconductor-insulator-superconductor (SIS) mixers and behaves as a single sideband receiver (SSB), providing a spectral resolution of 122 kHz and a total bandwidth of 1 GHz. The telescope was used in raster scan mode. Observing conditions were not optimal, which prevented us from acquiring the initially proposed observations with a signal-to-noise ratio (S/N) of 100 (5.5 h). Instead, data were acquired with an on-source integration time of 31 min, and an average S/N of only ≈8. Titan was observed near the western or eastern elongations at separation angles from Saturn of greater than 120″. Pointing and focusing of the telescope were regularly checked by scanning across Saturn in azimuth and in elevation (APEX has a pointing accuracy of 2″ rms over the sky). The beam size of APEX at 352 GHz is 17.3″. The apparent diameter of Titan was around 0.8″.

2.2. IRAM observations

HCN (3-2) at 265.9 GHz was observed on Titan with the IRAM 30-m and the Heterodyne Receiver Array (HERA) receiver on March 19, 2011[2]. The receiver also employs SIS mixers, and provides a spectral resolution of 4 MHz and a total bandwidth of 4 GHz. Observations were taken under good weather conditions ($\tau < 0.13$; PWV < 2.5 mm); the system temperature was 420 K. The telescope was used in wobbler-switch mode. The on-source integration time was 92 min, allowing us to acquire a spectrum with S/N = 36. The beam size of IRAM-30m at 260 GHz is 9.5″. The apparent diameter of Titan was also around 0.8″.

2.3. Data reduction

The observations were reduced using the Continuum and Line Analysis Single-dish Software (CLASS) package of the Grenoble Astrophysics Group[3]. CLASS follows standard data reduction processes for single-dish heterodyne spectroscopy; see for example Prestage et al. (2000), Pety (2005), and Polehampton & Hafok (2013).

3. Radiative transfer modelling, retrieval of parameters, and results

We computed the emerging radiance using a forward model described in Jarchow & Hartogh (1995), Jarchow (1998), and Hartogh & Jarchow (2004). This model was successfully applied to planetary spectra including those of Venus and Mars (Rengel et al. 2008; Hartogh et al. 2010). For Titan, the model consists of a line-by-line radiative transfer model that takes into consideration a homogeneous spherically symmetric atmosphere of Titan (grid of 127 altitude points ranging from 0 to 1500 km). We integrated the intensity of outgoing radiation across the disk and limb of the planet to obtain total flux at each frequency.

Abundances of the main atmospheric molecules were adopted following Niemann et al. (2010): 0.984, 0.001, and 0.014 for N_2, H_2, and CH_4, respectively. The main opacity sources at the frequencies of the HCN lines considered here are collision-induced absorption (CIA) due to N_2–N_2, which we took from Borysow & Frommhold (1986). We also checked the impact of other CIAs, in particular those due to N_2–CH_4 and N_2–H_2, and found them to be negligible. The transition parameters for both lines were taken from the 2016 edition of the high-resolution transmission molecular absorption (HITRAN) database (Gordon et al. 2017).

Regarding the vertical temperature–pressure (T-P) structure of Titan's atmosphere, we adopted the distribution used by Moreno et al. (2012) and Rengel et al. (2014), which is a combination of the Huygens Atmospheric Structure Instrument (HASI) profile (Fulchignoni et al. 2005) below 140 km, and the Cassini/Composite InfraRed Spectrometer (CIRS) stratospheric temperatures (Vinatier et al. 2010) above 140 km.

For the initial vertical distribution of HCN, we adopted the result of Marten et al. (2002) obtained from millimetre observations at IRAM, which is a well-probed reference distribution.

[1] This publication is based on data acquired with the Atacama-Pathfinder Experiment (APEX) under program ID 085.C-0910(A). APEX is a collaboration between the Max-Planck- Institut für Radioastronomie, the European Southern Observatory, and the Onsala Space Observatory.

[2] This work is based on observations carried out under project number [145-10] with the IRAM 30-m telescope. IRAM is supported by INSU/CNRS (France), MPG (Germany) and IGN (Spain).

[3] http://www.iram.fr/IRAMFR/GILDAS

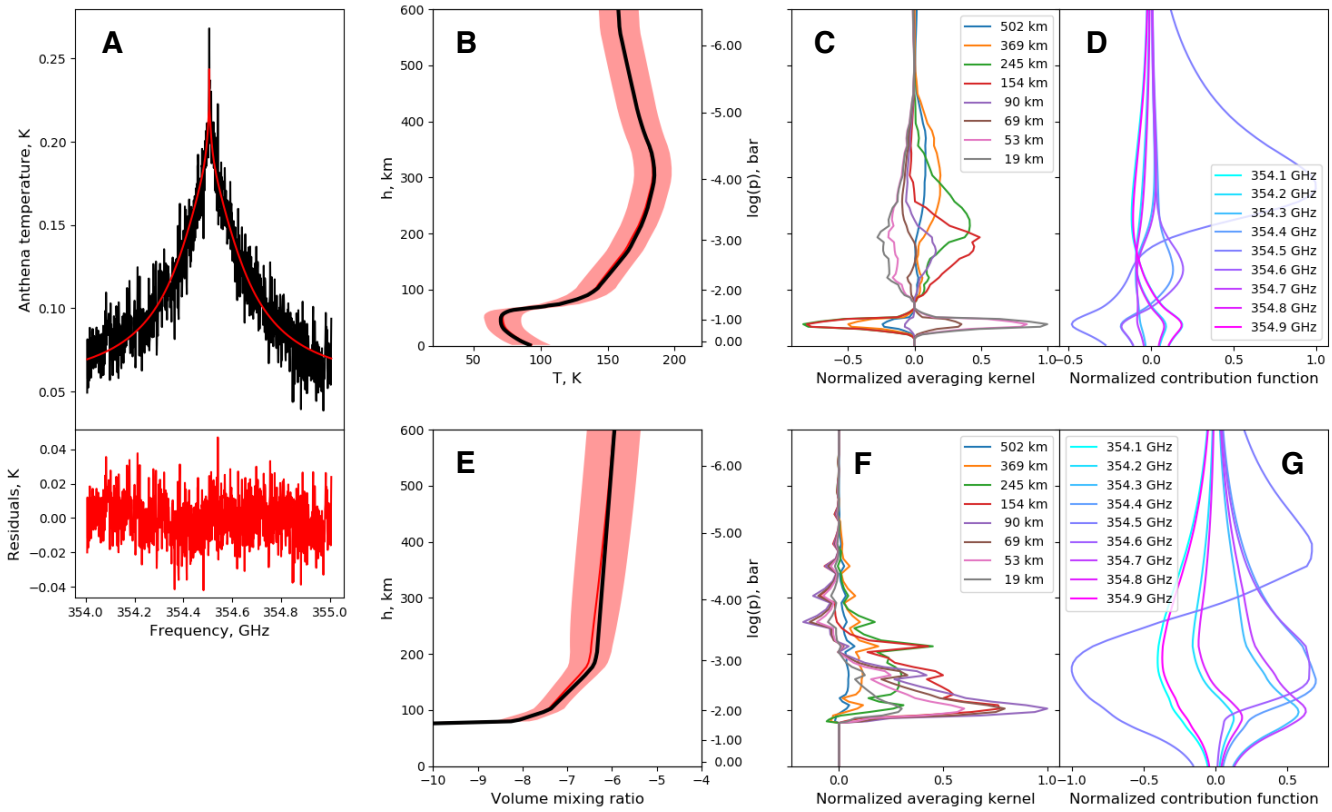

Fig. 1. *A*: comparison between observed and best-fit simulated HCN (4-3) lines (black and red, respectively, upper panel), and the difference between the observed and fitted spectra (lower panel). *B*: retrieved temperature. *C*: corresponding averaging kernels. *D*: corresponding normalised contribution functions. *E*: HCN distribution derived from the spectrum. *F*: corresponding averaging kernels. *G*: corresponding normalised contribution functions. In (B) and (E), the black and red lines show the initial and retrieved profiles, respectively, and the pink shadow shows the error bars. AVKs and contribution functions are shown for selected altitudes and frequencies, respectively, for better representation (see plot legends).

Its use offers a reliable result in conjunction with the data quality achieved with our observations, and has also been successfully applied to *Herschel*/SPIRE and PACS observations (Courtin et al. 2011; Rengel et al. 2014), which also facilitates inter-comparisons.

The fitting of the APEX and IRAM 30-m spectra by the models and the retrieval of the temperature and HCN vertical profiles from the spectral data are achieved by successive iterations using an optimal estimation (OE) algorithm. The key idea of the OE algorithm is to retrieve the atmospheric state from the spectra by searching for the solution that provides an optimal balance between how well the model fits the data and the deviation of model parameters from their expected values. A detailed description of the OE algorithm is given by Rodgers (1976). The OE algorithm implemented here is a PYTHON package presented in Shulyak et al. (2019).

Neither of the HCN lines reaches a well-defined continuum level. The temperature scale of the modelled spectra was in units of flux density S_ν. In order to compare the model with APEX observations, S_ν was converted to antenna temperature T_a using $S_\nu = 24.4 \times T_\mathrm{a} \cdot \eta_\mathrm{f}/\eta_\mathrm{a}$, where η_f and η_a are the forward and aperture efficiencies, respectively. In this study, we adopt the values considering the efficiencies listed on the APEX website[4]: η_a is 60 and η_f is 0.97 for 352 GHz. These values are expected to have a 10% uncertainty. In order to compare the model with IRAM observations, S_ν was converted to antenna temperature T_a. The relation between antenna temperature T_a and flux density S_ν for IRAM is expressed as $S_\nu = T_\mathrm{a}/\Gamma$, where Γ is the point source sensitivity of the antenna at 260 GHz[5]: 8.4.

3.1. Best-fitting solution

Figures 1 and 2 present the observations and show the best-fit between observed and modelled spectra, the difference between the two spectra (spectral residual), the temperature and HCN retrieval results, the corresponding averaging kernel functions (AVKs) and contribution functions D_y as defined by Rodgers (1990). Each AVK represents the sensitivity of the retrieval at a given altitude to variations in the true atmospheric state at all altitudes. Each contribution function shows how each channel contributes to the overall solution profile due to the measured intensity. The vertical information content is given by the AVK functions where their amplitudes are different from zero. At these altitudes, our retrieval is sensitive to the true profile. Results suggest that our retrievals are sensitive in the vertical ranges of ~50–480 km and 80–250 km for T and the mixing ratio for HCN (4-3), respectively, and ~50–550 km and 80–250 km for T and the mixing ratio for HCN (3-2), respectively.

The forward models (Figs. 1 and 2) show very good agreement with both observed HCN lines. Both instruments perform well which allows us to constrain HCN abundance. The HCN abundance retrieved from IRAM data is more accurate than the one from APEX data. In particular, the APEX data can be

[4] http://www.apex-telescope.org/telescope/efficiency

[5] https://www.iram.es/IRAMES/mainWiki/Iram30mEfficiencies

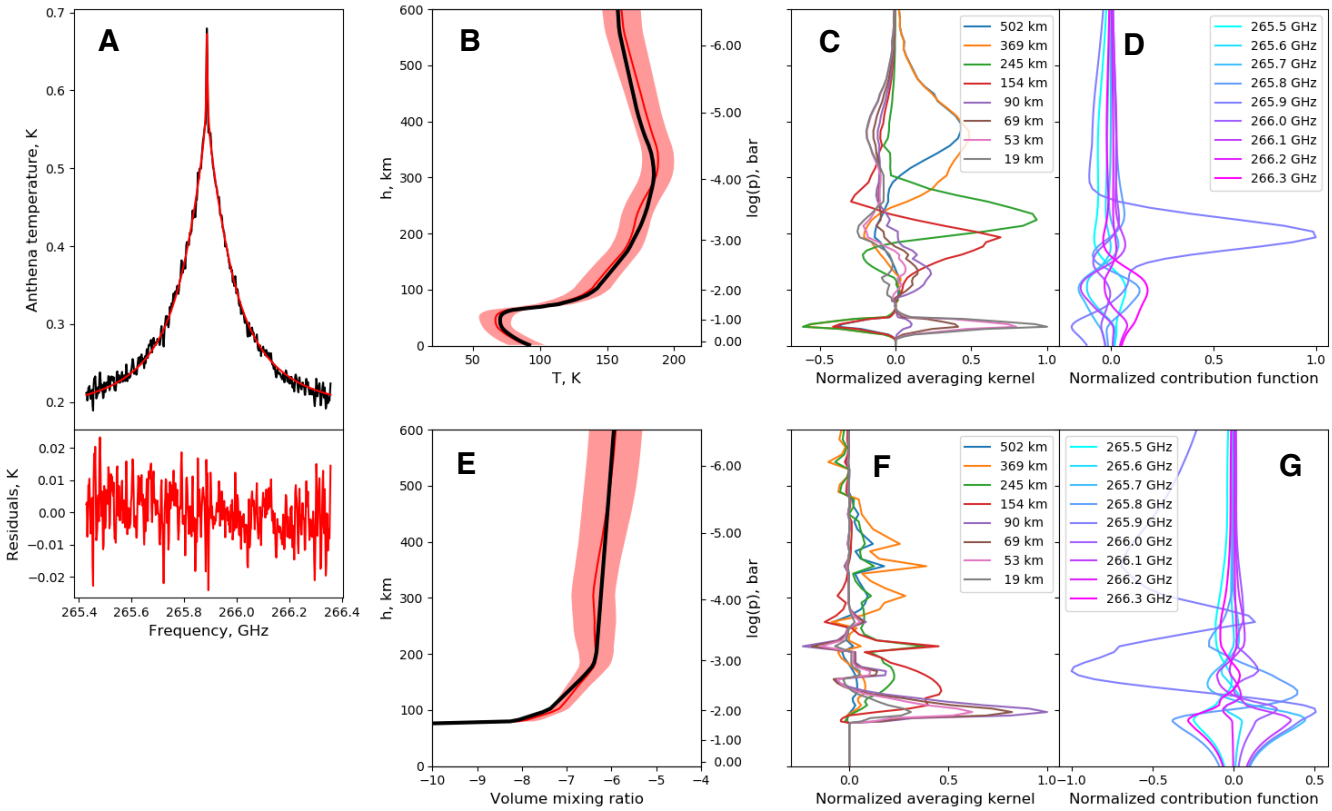

Fig. 2. Same as Fig. 1, but for the HCN (3–2) line.

satisfactorily fit with the model considering the profile of Marten et al. (2002). However, for IRAM data, we find that the retrieved HCN profile differs by a maximum factor of 2.5 from the reference profile of Marten et al. (2002) at altitudes of between 80 and 250 km, and the temperature differs by about 10 K from the adopted profile, both within the extent of the error bars. We therefore conclude that our retrievals are consistent with the profile of Marten et al. (2002). Both lines allow us to retrieve limited altitude information range, meaning that the abundance of HCN cannot be constrained by the data below 80 km and above 250 km.

3.2. Sensitivity of HCN retrievals to HCN a priori

Retrievals of trace gas concentrations is a mathematically ill-posed problem and has non-unique solutions. There is potentially a family of solutions, with ones that are physically meaningful and others that are not, both being able to fit the spectrum equally well within the same error range. To check the reliability of the best-fit solution, we briefly investigate the sensitivity of the retrieval to the chosen a priori solution. If there is sufficient information available in a spectrum to constrain atmospheric properties, the result should not be affected by the a priori atmospheric state. We retrieved HCN using three different a priori profiles to show that the retrieved HCN converges to a reproducible profile in the altitude range covered by the measurements, that is, to a robust profile. Figures 3 and 4 show an example of this test, that is, the results of retrievals assuming initial HCN constant profiles with altitude, with mixing ratios of $10^{-8} \pm 10^{-7}$, $10^{-7} \pm 10^{-6}$, and $10^{-6} \pm 10^{-5}$, respectively. We considered the reference temperature profile as described above with an associated uncertainty of 15 K.

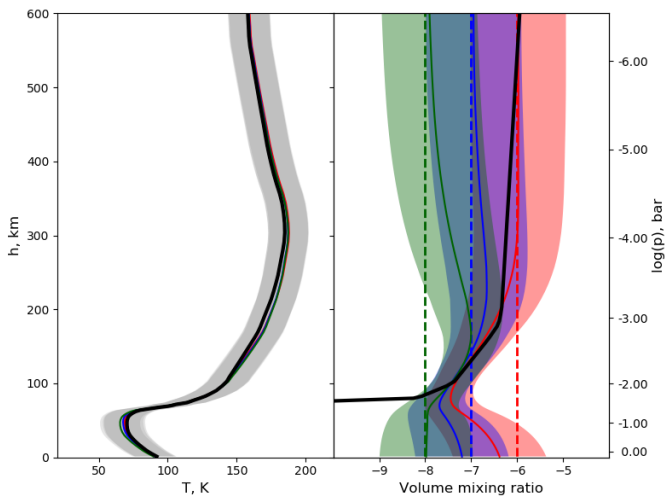

Fig. 3. Comparisons of retrieved temperature and HCN profiles from a range of three different a priori modified HCN profiles for the case of the APEX data. *Left*: reference temperature shown in solid black, and retrieved temperatures in solid coloured lines. An associated temperature uncertainty at 15 K is shown by the shadowed area. *Right*: different lines show a priori HCN profiles (dashed) corresponding retrieved HCN profiles (solid) and their errors (shadowed area). The HCN profile of Marten et al. (2002) is shown in solid black.

For the IRAM observations (Fig. 4), the retrieved HCN profiles share a common shape in the 80–180 km altitude region, where retrieval results are reported, demonstrating the validity of the HCN retrieval over this range. The retrievals from APEX data (Fig. 3) are less accurate and are only robust in a

Table 1. Summary of constrained altitude ranges.

Data	T sensitivity range (km)	HCN sensitivity range (km)	Altitude range where HCN is robustly retrieved (km)
APEX HCN (4-3)	50–480	80–250	100–150
IRAM-30m HCN (3-2)	50–550	80–250	80–180

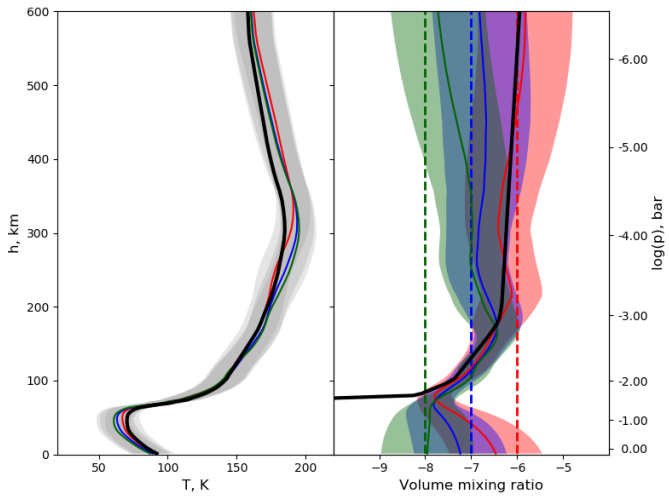

Fig. 4. Same as Fig. 3, but for the case of the IRAM data.

narrower altitude range of 100–150 km compared to the IRAM case, mostly because of the rather poor S/N of the APEX data.

The retrieved temperature profiles are very close to the initially assumed profile, with a maximum deviation of about 10 K in the case of IRAM data. We also tried to consider different temperature profiles as our initial guess (e.g. isothermal ones) in order to assess the temperature sensitivity of the HCN lines. However, in all these cases, we failed to find a converged solution using APEX data. For the IRAM data, our retrieved temperatures were very different from the adopted profile, and HCN abundance was found to vary drastically from one retrieval to another. Although these solutions provided fits to the observed HCN line of similar quality, we considered them non-physical and therefore excluded them from the current analysis; they are not shown here.

We show with this test that even considering the simplest possible HCN profile assumption, namely constant HCN profiles throughout the atmosphere, the measurements still allow us to retrieve HCN profiles of similar shapes as the profiles derived with non-constant profiles. All our calculations show that the derived HCN profiles are very close (within the error bars) to that provided by Marten et al. (2002). We conclude here that the choice of the first guess has only a minimal effect on the retrieval results over the levels probed by the measurements and that the data can constrain an unbiased atmospheric structure within that range. A summary of the altitude heights probed by the measurements for T and mixing ratios and where HCN is robustly retrieved is given in Table 1.

4. Discussion

In Fig. 5, we present results of comparisons of HCN from APEX, IRAM30-m, and *Herschel*. In particular, we show the HCN mean profile obtained by considering four observations acquired quasi-simultaneously, and illustrate the associated 1-σ standard deviation of the mean differences between the profiles. The HCN profiles derived here from the ground are in agreement with the findings from *Herschel*. Our analysis confirms the result of Marten et al. (2002) from whole-disk mm observations. The four data sets show good agreement in shape and amounts of HCN, especially above 80 km and below 250 km. In this altitude range, there is a maximum difference of 2.5 ppm in the amount of HCN.

The inferred abundances here are also consistent with the vertical distribution found in previous observational studies (Fig. 6). The mean profile that we derive here is consistent with those derived from the Atacama Large Millimeter/submillimeter Array (ALMA) (Thelen et al. 2019; Molter et al. 2016; Lellouch et al. 2019) and Cassini/CIRS, both from limb observations at 80° N (Vinatier et al. 2007) and from nadir observations inferred near the equator to altitudes of around 130 km (Coustenis et al. 2007). However, the abundance increase with altitude is less steep than in the Submillimeter Array (SMA)-derived profiles (Gurwell 2004) above ~230 km. Above 250 km, where our observations start to lose sensitivity, we find that our HCN profile is consistent with the previous observations of Vinatier et al. (2007) and the photochemical model of Loison et al. (2015). Furthermore, our mean HCN profile is also comparable to the photochemical models of Krasnopolsky (2014) and Vuitton et al. (2019) below 230 km. The HCN modelled profiles by Loison et al. (2015), Dobrijevic & Loison (2018), and Lora et al. (2018) appear to have over-predicted the amounts of HCN in atmospheres below 170 km. However, the earlier ones are consistent in shape. These photochemistry models require revision, not only in the calculated absolute amount of HCN, but also in its vertical distribution below 170 km and 250 km, and, excluding Loison et al. (2015), above 400 km as well. The model from Lora et al. (2018) includes HCN modelled in the atmospheres of planets around G stars, with planetary parameters corresponding to Titan (more details in Sect. 5).

Figure 6 shows that measured HCN abundances on Titan with data acquired from space and the ground at similar epochs and with different transitions exhibit similar abundance distributions, and confirms that the former data set shows a small difference with respect to the ground-based observations, with a difference that is essentially consistent and depends on the altitude level. This inter-validation allows us to derive reliable and consistent measurements. Beyond the intrinsic scientific interest, these observations prove their usefulness in supporting spacecraft observations of Solar System bodies, and in particular, of Titan's atmosphere.

We note that for the inter-comparisons presented here, we do not discuss the possible systematic effects due to different instruments and retrieval procedures. The impact of these latter in the comparisons are beyond the scope of this paper. Regarding possible temporal variability effects in Titan's atmosphere, the mean profile derived in this study confirms that the disk-averaged HCN does not vary significantly at these altitudes in

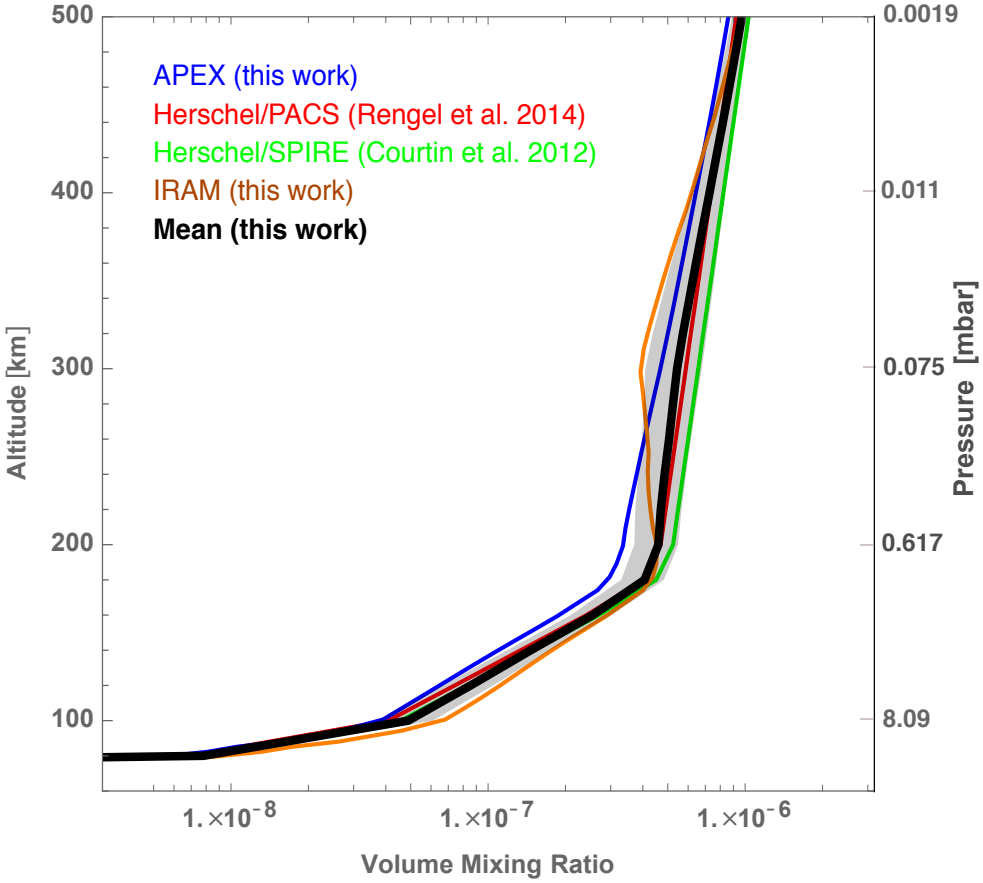

Fig. 5. Vertical distributions of HCN obtained with APEX and IRAM 30-m (blue and yellow, respectively) compared with the *Herschel* profiles obtained by Courtin et al. (2011) and Rengel et al. (2014) (green and red, respectively). The black distribution shows the mean profile obtained from the four datasets, and the shaded region shows the associated 1-σ standard deviation of the mean difference.

Titan's atmosphere between 2010 and 2011 (our observations), 2012 and 2015 (Thelen et al. 2019), and in 2016 (Lellouch et al. 2019). Furthermore, the disk-averaged temperature profiles of Titan obtained with ALMA were consistent within the error bars between 2012 and 2015 (Thelen et al. 2018), and were also consistent with the T–P profile used in this work, justifying its adoption here.

5. HCN in other planetary atmospheres

Other planets can be seen as diverse possible laboratories for atmospheric and prebiotic chemistry. Here, we summarise the main findings from the literature for HCN in planetary atmospheres relevant to our study. In the Solar System, HCN is also present in the atmospheres of Pluto, Neptune, and Uranus, at concentrations of ~40 ppm, ~1 ppb, and 0.1 ppb, respectively (Marten et al. 1993; Lellouch et al. 2017). HCN has been detected in Jupiter and upper limits of 0.93 ppb have been placed (Davis et al. 1997). Cool terrestrial worlds with dense, hazy, and chemically complex atmospheres, that is, Titan-like exoplanets, could exist around a wide range of host stars. In those atmospheres, there may be different chemical pathways leading HCN production and destruction, and these could be affected by variations in the far-to-near-ultraviolet ratio (FUV/NUV ratio). While the main formation and loss pathways of HCN in Titan's atmosphere have been widely studied (Loison et al. 2015; Pearce et al. 2020, and references therein), little is known for Titan-like exoplanets. Simulations of the atmospheric circulation and photochemistry of Titan-like exoplanets have been used to explore the sensitivity to host stellar type. It has been estimated that HCN mixing ratio profiles are similar between the different stellar spectra cases (G, K, and M stars) because HCN formation and loss are tied to the Lyman-α flux. HCN abundances are slightly higher for the K dwarf case due to the higher N abundances from increased flux or photons (Lora et al. 2018). Modelled HCN in the stellar spectra case G holds constant planetary parameters at values corresponding to Titan, and these latter authors run their code with a default HCN profile provided by Vinatier et al. (2007) and Lora et al. (2015). We find disagreement between our mean profile and the HCN-modelled profile from Lora et al. (2018). The HCN modelled profile appears to have over-predicted the amounts of HCN in atmospheres of planets around a G star; these appear to be 100 times too large below ~400 km, even though the two profiles are consistent in shape below ~400 km. The HCN-modelled profile from Lora et al. (2018) does not include the effects of condensation clouds, which are confined to the lower atmosphere. The inferred HCN results obtained here could be assimilated as default profiles into climate models and chemistry calculations.

Furthermore, simulations of the spectra of HCN in the IR have been found to display similar features considering the three different stellar cases mentioned here (Lora et al. 2018). The response to variations of further climate-relevant parameters could be explored in order to further interpret exoplanetary spectra, and to understand the key physical mechanisms shaping Titan-like exoplanetary atmospheres. Detailed simulations are beyond the scope of this paper.

HCN has been tentatively detected in the peculiar super-Earth 55 Cancri e with spectroscopic observations in the NIR (Tsiaras et al. 2016; Deibert et al. 2021) and in the hot Jupiter WASP-63b (MacDonald & Madhusudhan 2017) with data

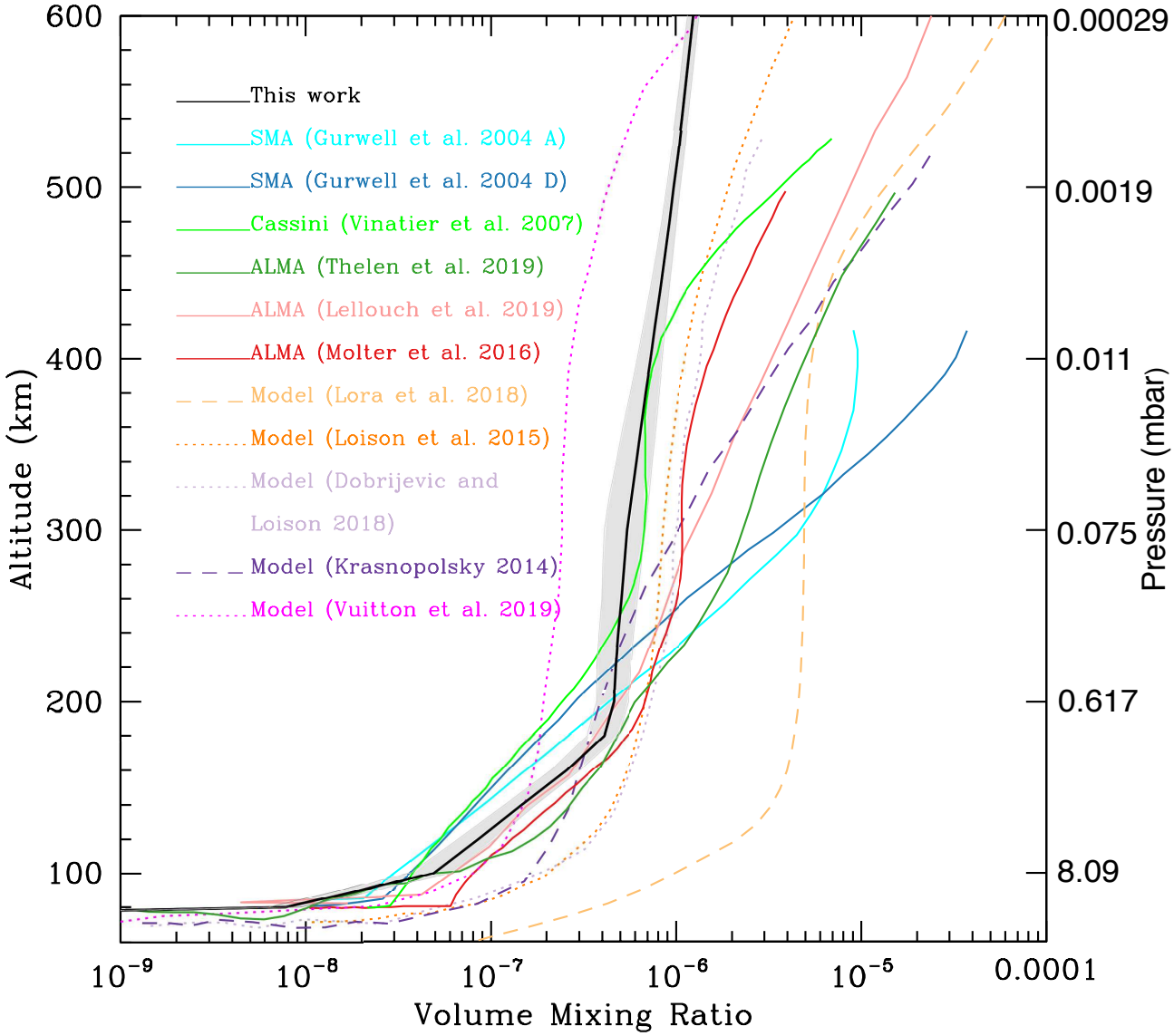

Fig. 6. Mean HCN profile derived here (black) compared to observed profiles from the literature (coloured solid lines), and to predicted HCN profiles from photochemical models for Titan (coloured dashed lines) and for the atmosphere of planets around G stars (Lora et al. 2018).

obtained with the *Hubble* Space Telescope, and its detectability with future missions to observe super-Earths has been explored (Miguel 2019). HCN may also be present in ultra-hot Jupiters. In such atmospheres, a substantial degree of thermal ionisation and clouds may drive lightning and creation of HCN by ion-neutral chemistry. HCN has been searched for in hot H_2 atmospheres with high-resolution spectroscopy, and an abundance of 10^{-5} has been considered, placing a minimum limit on the HCN mixing ratio of log(HCN) = −6.5 in the atmosphere of the Hot Jupiter HD 209458b (Hawker et al. 2018). Disequilibrium chemistry (vertical mixing) can enhance HCN abundances, dredging-up HCN to upper layers of the atmosphere and opening the possibility to detect it with future space-based facilities (Shulyak et al. 2020). HCN abundances in N_2–dominated atmospheres depend critically on the atmospheric C/O ratio, with significantly greater amounts of HCN generated photochemically when C/O ≥ 1 (Rimmer & Rugheimer 2019). Future data in the IR and dedicated space telescopes will help to shed more light on HCN in planetary atmospheres.

6. Conclusions

We carried out complementary APEX and IRAM 30-m HCN (4–3) and (3–2) line observations, respectively, in Titan's atmosphere around the times of *Herschel*/PACS and SPIRE observations, and measured the HCN abundance using a retrieval algorithm based on optimal estimation. The quality and coverage of these data are sufficient for us to make a precise determination of the HCN abundance in the atmosphere of Titan at altitudes of 100–150 km and 80–180 km from APEX and IRAM data, respectively. However, we note that the mixing ratio obtained from APEX data is less reliable than that derived from IRAM data because of the inferior data quality of the former.

Our main conclusions are as follows:

1. We performed a consistency check and assessed the accuracy of the *Herschel* HCN observations by comparing them with ground-based observations. The HCN vertical profiles that we infer in this work are consistent with *Herschel*/PACS and SPIRE profiles, confirming the previous determination

of Marten et al. (2002). Our retrieved HCN profiles are also consistent with the observed profiles from ALMA, Cassini/CIRS, and SMA (the latest ones below ~230 km). To the contrary, most HCN profiles that result from photochemical models display large deviations above 400 km with respect to that retrieved here.

2. This study is relevant to the scientific community because the *Herschel* observations are publicly available[6] and may be further used in future studies of Titan's atmosphere. Our analysis shows that, with the current lack of space-based instruments observing Titan, the submm ground-based telescopes can successfully help to fill the consequent gaps in available data.

3. Here we show that our HCN profiles can be used as reference between 80 and 250 km. For example, they could be used as input for modelling the atmospheres of hot super-Earths, as a guide to understanding what to expect in an N-dominated atmosphere, and as a reference in preparation for future observations of Titan and Titan-like exoplanets.

Observations of HCN with additional rotational lines – including rotational lines of isotopes – in Titan's atmosphere and a search for HCN in N-dominated atmospheres are required to provide additional insight in order to improve models of Titan and Titan-like exoplanets

Acknowledgements. M.R. and D.S. acknowledge the support by the DFG priority program SPP 1992 "Exploring the Diversity of Extrasolar Planets" (DFG PR 36 24602/41). D.S. acknowledges financial support from the State Agency for Research of the Spanish MCIU through the "Center of Excellence Severo Ochoa" award to the Instituto de Astrofísica de Andalucía (SEV-2017-0709). We thank Juan Lora for providing profiles for Titan-like planets around diverse stars. We thank the anonymous referee for the insightful comments and suggestions to the manuscript. We gratefully acknowledge the support of the APEX and IRAM staff during the observations. We acknowledge JPL's Horizons online ephemeris generator for providing Titan's position during the observations. This research has made use of NASA's Astrophysics Data System. PACS has been developed by a consortium of institutes led by MPE (Germany) and including UVIE (Austria); KU Leuven, CSL, IMEC (Belgium); CEA, LAM (France); MPIA (Germany); INAF-IFSI/OAA/OAP/OAT, LENS, SISSA (Italy); IAC (Spain). This development has been supported by the funding agencies BMVIT (Austria), ESA-PRODEX (Belgium), CEA/CNES (France), DLR (Germany), ASI/INAF (Italy), and CICYT/MCYT (Spain). SPIRE has been developed by a consortium of institutes led by Cardiff University (UK) and including Univ. Lethbridge (Canada); NAOC (China); CEA, LAM (France); IFSI, Univ. Padua (Italy); IAC (Spain); Stockholm Observatory (Sweden); Imperial College London, RAL, UCL-MSSL, UKATC, Univ. Sussex (UK); and Caltech, JPL, NHSC, Univ. Colorado (USA). This development has been supported by national funding agencies: CSA (Canada); NAOC (China); CEA, CNES, CNRS (France); ASI (Italy); MCINN (Spain); SNSB (Sweden); STFC, UKSA (UK); and NASA (USA).

References

Borysow, A., & Frommhold, L. 1986, ApJ, 311, 1043
Courtin, R., Swinyard, B. M., Moreno, R., et al. 2011, A&A, 536, L2
Coustenis, A., Bezard, B., Gautier, D., Marten, A., & Samuelson, R. 1991, Icarus, 89, 152
Coustenis, A., Achterberg, R. K., Conrath, B. J., et al. 2007, Icarus, 189, 35
Davis, G. R., Naylor, D. A., Griffin, M. J., Clark, T. A., & Holland, W. S. 1997, Icarus, 130, 387
Deibert, E. K., de Mooij, E. J. W., Jayawardhana, R., et al. 2021, ApJ, 161, 209
Dobrijevic, M., & Loison, J. C. 2018, Icarus, 307, 371
Fulchignoni, M., Ferri, F., Angrilli, F., et al. 2005, Nature, 438, 785
Gordon, I. E., Rothman, L. S., Hill, C., et al. 2017, J. Quant. Spec. Rad. Transf., 203, 3
Griffin, M. J., Abergel, A., Abreu, A., et al. 2010, A&A, 518, L3
Gurwell, M. A. 2004, ApJ, 616, L7
Güsten, R., Nyman, L. Å., Schilke, P., et al. 2006, A&A, 454, L13
Hartogh, P., & Jarchow, C. 2004, Proceedings of the International Workshop on Critical Evaluation of mm-/submm-wave Spectroscopic Data for Atmospheric Observations, eds. T. Amano, Y. Kasai, & T. Manabe, 158, 75
Hartogh, P., Błecka, M. I., Jarchow, C., et al. 2010, A&A, 521, L48
Hartogh, P., Lellouch, E., Moreno, R., et al. 2011, A&A, 532, L2
Hawker, G. A., Madhusudhan, N., Cabot, S. H. C., & Gandhi, S. 2018, ApJ, 863, L11
Hidayat, T., Marten, A., Bézard, B., et al. 1997, Icarus, 126, 170
Jarchow, C. 1998, PhD Thesis
Jarchow, C., & Hartogh, P. 1995, Proc. SPIE 2586, 196
Kovács, T., & Turányi, T. 2010, Icarus, 207, 938
Krasnopolsky, V. A. 2014, Icarus, 236, 83
Lara, L. M., Lellouch, E., López-Moreno, J. J., & Rodrigo, R. 1996, J. Geophys. Res., 101, 23261
Lellouch, E., Gurwell, M., Butler, B., et al. 2017, Icarus, 286, 289
Lellouch, E., Gurwell, M. A., Moreno, R., et al. 2019, Nat. Astron., 3, 614
Loison, J. C., Hébrard, E., Dobrijevic, M., et al. 2015, Icarus, 247, 218
Lora, J. M., Lunine, J. I., & Russell, J. L. 2015, Icarus, 250, 516
Lora, J. M., Kataria, T., & Gao, P. 2018, ApJ, 853, 58
MacDonald, R. J., & Madhusudhan, N. 2017, ApJ, 850, L15
Marten, A., Gautier, D., Owen, T., et al. 1993, ApJ, 406, 285
Marten, A., Hidayat, T., Biraud, Y., & Moreno, R. 2002, Icarus, 158, 532
Miguel, Y. 2019, MNRAS, 482, 2893
Molter, E. M., Nixon, C. A., Cordiner, M. A., et al. 2016, AJ, 152, 42
Moreno, R., Lellouch, E., Lara, L. M., et al. 2012, Icarus, 221, 753
Niemann, H. B., Atreya, S. K., Demick, J. E., et al. 2010, J. Geophys. Res. (Planets), 115, E12006
Pearce, B. K. D., Molaverdikhani, K., Pudritz, R. E., Henning, T., & Hébrard, E. 2020, ApJ, 901, 110
Pety, J. 2005, SF2A-2005: Semaine de l'Astrophysique Francaise, 721
Pilbratt, G. L., Riedinger, J. R., Passvogel, T., et al. 2010, A&A, 518, L1
Poglitsch, A., Waelkens, C., Geis, N., et al. 2010, A&A, 518, L2
Polehampton, E., & Hafok, H. 2013, APEX-MPI-MAN-0012
Prestage, R., Meyerdierks, H., Lightfoot, J., et al. 2000, Starlink User Note, 17
Rengel, M., Hartogh, P., & Jarchow, C. 2008, Planet. Space Sci., 56, 1368
Rengel, M., Sagawa, H., & Hartogh, P. 2011, Adv. Geosci, 25: Planet. Sci. (PS), 25, 173
Rengel, M., Sagawa, H., Hartogh, P., et al. 2014, A&A, 561, A4
Rimmer, P. B., & Rugheimer, S. 2019, Icarus, 329, 124
Rodgers, C. D. 1976, Rev. Geophys. Space Phys., 14, 609
Rodgers, C. D. 1990, J. Geophys. Res., 95, 5587
Sekine, Y., Genda, H., Sugita, S., Kadono, T., & Matsui, T. 2011, Nat. Geosci., 4, 359
Shulyak, D., Rengel, M., Reiners, A., Seemann, U., & Yan, F. 2019, A&A, 629, A109
Shulyak, D., Lara, L. M., Rengel, M., & Nèmec, N. E. 2020, A&A, 639, A48
Thelen, A. E., Nixon, C. A., Chanover, N. J., et al. 2018, Icarus, 307, 380
Thelen, A. E., Nixon, C. A., Chanover, N. J., et al. 2019, Icarus, 319, 417
Tsiaras, A., Rocchetto, M., Waldmann, I. P., et al. 2016, ApJ, 820, 99
Vassilev, V., Meledin, D., Lapkin, I., et al. 2008, A&A, 490, 1157
Vinatier, S., Bézard, B., & Nixon, C. A. 2007, Icarus, 191, 712
Vinatier, S., Bézard, B., Nixon, C. A., et al. 2010, Icarus, 205, 559
Vuitton, V., Yelle, R. V., Klippenstein, S. J., Hörst, S. M., & Lavvas, P. 2019, Icarus, 324, 120
Wilson, E. H., & Atreya, S. K. 2004, J. Geophys. Res. (Planets), 109, E06002

[6] http://archives.esac.esa.int/hsa/whsa/